THE JOURNAL OF PHYSICAL CHEMISTRY A
A JOURNAL OF THE AMERICAN CHEMICAL SOCIETY

pubs.acs.org/JPCA Article

Fulvenallenyl Radical ($C_7H_5^{\cdot}$)-Mediated Gas-Phase Synthesis of Bicyclic Aromatic $C_{10}H_8$ Isomers: Can Fulvenallenyl Efficiently React with Closed-Shell Hydrocarbons?

Alexander M. Mebel,*[,∇] Wang Li,[∇] Luna Pratali Maffei,* Carlo Cavallotti, Alexander N. Morozov, Chang-Yang Wang, Jiu-Zhong Yang, Long Zhao,* and Ralf I. Kaiser*

Cite This: J. Phys. Chem. A 2024, 128, 5707−5720 Read Online

ABSTRACT: To understand the reactivity of resonantly stabilized radicals, often found in relevant concentrations in gaseous environments, it is important to determine their main reaction pathways. Here, it is investigated whether the fulvenallenyl radical ($C_7H_5^{\cdot}$) reacts preferentially with closed-shell molecules or radicals. Electronic structure calculations on the $C_{10}H_9$ potential energy surface accessed by the reactions of $C_7H_5^{\cdot}$ with methylacetylene (CH_3CCH) and allene (H_2CCCH_2) were combined with RRKM-ME calculations of temperature- and pressure-dependent rate constants using the automated EStokTP software suite and kinetic modeling to assess the reactivity of $C_7H_5^{\cdot}$ with closed-shell unsaturated hydrocarbons. Experimentally, the reactions were attempted in a chemical microreactor heated to 998 ± 10 K by preparing fulvenallenyl radicals via pyrolysis of trichloromethylbenzene ($C_7H_5Cl_3$) and seeding the radicals in methylacetylene or allene carrier gas, with product identification by means of photoionization mass spectrometry. The measured photoionization efficiency curve of m/z = 128 was assigned to a linear combination of the reference curves of two $C_{10}H_8$ isomers, azulene (minor) and naphthalene (major), presumably resulting from the $C_7H_5^{\cdot}$ plus C_3H_4 reactions. However, the calculations demonstrated that these reactions are too slow, and kinetic modeling of processes in the reactor allowed us to conclude that the observation of naphthalene and azulene is due to the $C_7H_5^{\cdot}$ plus $C_3H_3^{\cdot}$ reaction, where propargyl is produced by direct hydrogen atom abstraction by chlorine (Cl) atoms from allene or methylacetylene and Cl stem from the pyrolysis of $C_7H_5Cl_3$. Modeling results under the copyrolysis conditions of toluene and methylacetylene in high-temperature shock tube experiments confirmed the prevalence of the fulvenallenyl reaction with propargyl over its reactions with C_3H_4 even when the concentrations of allene and methylacetylene largely exceed that of propargyl. Overall, the reactions of fulvenallenyl with both allene and methylacetylene were found to be noncompetitive in the formation of naphthalene and azulene thus attesting the inefficiency of the fulvenallenyl radical reactions with the prototype closed-shell hydrocarbon species. In the meantime, the new reaction pathways revealed, including H-assisted isomerizations between $C_{10}H_8$ isomers and decomposition reactions of various $C_{10}H_9$ isomers, emerge as relevant and are recommended for inclusion in combustion kinetic models for naphthalene formation.

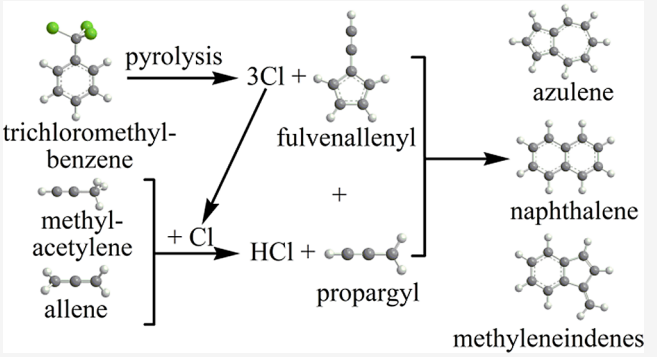

1. INTRODUCTION

Recent kinetic modeling studies[1−4] based upon flame-sampling and jet stirred reactor pyrolysis experiments strongly indicate that a highly resonantly stabilized free radical fulvenallenyl ($C_7H_5^{\cdot}$), which was first proposed by da Silva and Bozzelli as a combustion intermediate,[5] can play a significant role in the gas-phase synthesis of the prototype two-ring polycyclic aromatic hydrocarbon (PAH) naphthalene ($C_{10}H_8$). The emergence of naphthalene sets off the growth of PAHs in combustion flames eventually leading to the formation of soot. PAH molecules represent critical precursors not only to soot in combustion systems[6−9] but also to carbonaceous nanoparticles in circumstellar envelopes of carbon-rich asymptotic giant branch (AGB) stars,[10,11] where they are considered as viable carriers of diffuse interstellar bands (DIBs),[12,13] i.e., absorption features superimposed on the interstellar extinction curve from the blue visible (400 nm) to the near-infrared (1.2 mm) region of the electromagnetic spectrum. Naphthalene can be formed through many different pathways[14,15] verified both by experiments and theory and included in the current kinetic

Received: April 11, 2024
Revised: June 8, 2024
Accepted: June 27, 2024
Published: July 5, 2024

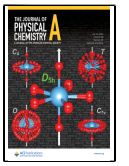

https://doi.org/10.1021/acs.jpca.4c02386
J. Phys. Chem. A 2024, 128, 5707−5720

models of the PAH growth, such as hydrogen abstraction−acetylene addition (HACA)[16−20] and hydrogen abstraction−vinylacetylene addition (HAVA)[21,22] commencing from benzene, self-recombination of the cyclopentadienyl radical ($C_5H_5^{\cdot} + C_5H_5^{\cdot}$),[23−27] recombination of benzyl and propargyl radicals ($C_7H_7^{\cdot} + C_3H_3^{\cdot}$)[28,29] and of indenyl with methyl ($C_9H_7^{\cdot} + CH_3^{\cdot}$).[30,31] Still, the models tend to perform poorly and inconsistently in regard to naphthalene predictions. For instance, C3MechV3.3 and CRECK kinetic models tend to underpredict naphthalene formation in ethylene, acetylene, and benzene premixed flames, especially at lower pressures,[32,33] as well as in flow reactor experiments of cyclopentadiene and benzene oxidation. Conversely, naphthalene formation in counterflow diffusion flames of various fuels such as acetylene, ethylene, and butene is generally overpredicted also in other literature models.[34] Especially in acetylene and ethylene flames, the interaction between C7 and C3 species (e.g., benzyl, fulvenallenyl, propargyl, propyne, and allene) is key to naphthalene growth.[34] Therefore, a more comprehensive inclusion of "C7" aromatic chemistry is required for the improvement,[35] where fulvenallenyl, along with benzyl, vinylcyclopentadienyl, and tropyl represent crucial intermediates.

The fulvenallenyl radical can be produced by direct hydrogen abstraction from or through the pyrolysis of fulvenallene (C_7H_6)[36−38] at elevated temperatures, as in combustion flames and in circumstellar envelopes close to the central star or via photolysis of the C−H bond by the internal ultraviolet field existing even deep inside molecular clouds. In turn, C_7H_6 is the predominant product of unimolecular decomposition of benzyl[39,40] and may also be formed in the $C_6H_6 + CH^{\cdot}$,[38] $C_5H_5^{\cdot} + C_2H_2$,[40] and $C_6H_6 + C(^3P)$[39] reactions; this molecule has been recently detected in the Taurus Molecular Cloud-1 (TMC-1)[41] with a relatively high fractional abundance of $(8.7 \pm 0.7) \times 10^{-9}$. Alternatively, in combustion flames, fulvenallenyl can be formed through isomerization/dehydrogenation of the benzyl radical, through the growth reaction of propargyl with diacetylene,[42] and via oxidation reactions of phenylacetylene.[43] Due to its high stability owing to the radical delocalization, $C_7H_5^{\cdot}$, if not removed by oxidation, can accumulate and enter reactions with other available molecules and radicals, resulting in the hydrocarbon growth. Very recently, the reaction of fulvenallenyl ($C_7H_5^{\cdot}$) with another resonantly stabilized radical propargyl ($C_3H_3^{\cdot}$) was carried out within a chemical microreactor and resulted in the gas-phase synthesis of two bicyclic aromatic $C_{10}H_8$ isomers, naphthalene and azulene, as evidenced through photoionizing the reaction products by tunable vacuum ultraviolet (VUV) light.[44]

Here, we explore experimentally and computationally to what degree the gas-phase reaction of the resonantly stabilized fulvenallenyl radical ($C_7H_5^{\cdot}$) with allene (H_2CCCH_2) and methylacetylene (CH_3CCH) competes with the fulvenallenyl ($C_7H_5^{\cdot}$)—propargyl ($C_3H_3^{\cdot}$) system in the preparation of the 10π-Hückel aromatic $C_{10}H_8$ isomers−fundamental molecular building blocks in molecular mass growth processes of carbonaceous nanostructures.[43,45−47] Formed through ring annulation within a high-temperature chemical microreactor,[48] the reaction products were entrained in a supersonic molecular beam and analyzed isomer-specifically via fragment-free photoionization of the neutral products exploiting tunable VUV light in conjunction with a reflection time-of-flight mass spectrometer (Re-TOF-MS).[49] We performed electronic structure calculations on the pertinent potential energy surface (PES), followed by the evaluation of the reaction rate constants and kinetic modeling of the physicochemical processes in the reactor. Our studies reveal that naphthalene ($C_{10}H_8$) along with its fulvalene and azulene isomers originate from the reaction of the fulvenallenyl radical ($C_7H_5^{\cdot}$) with the propargyl radical ($C_3H_3^{\cdot}$) with the latter formed through efficient hydrogen abstraction by atomic chlorine−the atomic fragment generated via the pyrolysis of the trichloromethylbenzene precursor ($C_7H_5Cl_3$) of the fulvenallenyl radical ($C_7H_5^{\cdot}$)—rather than from the reactions with allene and methylacetylene (C_3H_4). Then, we confirmed that this behavior also persists when the concentrations of allene and methylacetylene largely prevail over those of propargyl radical, i.e., during the copyrolysis of toluene and methylacetylene in the shock tube experiments of Sun et al.[50] In this latter case, the molecular addition pathway still contributed less, by 2 orders of magnitude, than the radical recombination pathway, despite the high concentrations of the C_3H_4 species. Overall, the reactions of the fulvenallenyl radical ($C_7H_5^{\cdot}$) with both allene and methylacetylene were found to be noncompetitive in the formation of naphthalene and azulene, thus attesting the inefficiency of the fulvenallenyl radical reactions with these prototype closed-shell hydrocarbon species.

2. EXPERIMENTAL METHODS

The experiments were carried out at the Combustion and Flame Endstation of the National Synchrotron Radiation Laboratory (NSRL).[44,49] Briefly, a continuous molecular beam of fulvenallenyl radicals ($C_7H_5^{\cdot}$) was prepared in situ via the pyrolysis of the trichloromethylbenzene precursor ($C_7H_5Cl_3$, Aladdin, > 99%) within a resistively heated silicon carbide (SiC) tube at 998 ± 10 K.[44] This precursor was kept in a stainless-steel bubbler at 283 K and entrained in helium (He, Kunshan Air Liquide Gas Technology Inc., > 99.999%) as regulated by a mass flow controller (MKS, Andover, MA, USA). The trichloromethylbenzene-helium gas mixture was further mixed with the hydrocarbon reactants (experiment I: methylacetylene, CH_3CCH, Dalian Special Gases Co., Ltd., > 99%, 0.15 mL min^{-1}; experiment II: allene, H_2CCCH_2, Dalian Special Gases Co., Ltd., > 99%, 0.15 mL min^{-1}). The total pressure of 300 Torr was monitored by a pressure sensor (PMS 111, BD Sensor Co., Ltd.). The continuous supersonic molecular beam containing the reactants and products formed after the gas mixture passed through a stainless-steel nozzle with a 0.1 mm aperture, entered the microreactor and supersonically expanded through a 2.0 mm diameter nickel skimmer located 10.0 mm downstream of the pyrolytic reactor. The quasi-continuous tunable synchrotron VUV light crossed the supersonic molecular beam and photoionized a fraction of the entrained species. The ions were then collected by a microchannel plate (MCP) detector in a Re-TOF-MS.[51−53] Control experiments were also performed under identical experimental conditions by simply replacing allene or methylacetylene with nonreactive helium gas. Photoionization efficiency (PIE) curves, which report ion counts of well-defined mass-to-charge (m/z) ratios versus the photon energy, were extracted from the mass spectra recorded over the photon energy range from 7.20 to 9.00 eV in an interval of 0.05 eV.

https://doi.org/10.1021/acs.jpca.4c02386
J. Phys. Chem. A 2024, 128, 5707−5720

3. COMPUTATIONAL METHODS

The PESs for the fulvenallenyl radial ($C_7H_5^{\cdot}$) reactions with allene and methylacetylene (C_3H_4) were explored using the EStokTP software code[54] in conjunction with the Gaussian 09[55] and MRCC[56,57] quantum chemistry packages. H atom abstraction reactions from the C_3H_4 isomers by the fulvenallenyl radical were also explored with the same methodology. Here, geometry optimization of all stationary structures, including bimolecular reactants and products, intermediates, and transition states, was performed employing the ωB97X-D dispersion-corrected range-separated hybrid functional[58] within density functional theory (DFT) with the 6-311G(d,p) basis set. Vibrational frequencies were evaluated at the same ωB97X-D/6-311G(d,p) level of theory. EStokTP automatically identified internal rotors in molecular structures and carried out geometry optimization after random sampling of the dihedral angles corresponding to internal rotations. This procedure ensured that the lowest energy conformation of each isomer or transition state was identified. The optimizations were followed by one-dimensional scans of the hindered rotor potentials also performed at the ωB97X-D/6-311G(d,p) level, and then a reduced number of vibrational frequencies were recomputed, projecting the internal rotors out. The package automatically determines the symmetry number for each isomer or transition state. Single-point energies were refined using the FNO−CCSD(T) approach[59] implemented in the MRCC package with the cc-pVTZ-F12 and cc-pVQZ-F12 basis sets,[60] with extrapolation of the total high-level energy to the complete basis set limit, $E(\mathrm{CBS}) = E(\mathrm{VQZ}) + 0.69377*[E(\mathrm{VQZ}) - E(\mathrm{VTZ})]$.[61] The FNO−CCSD(T)/CBS relative energies should be accurate within 4 kJ mol^{-1} or better.[59]

The EStokTP package generated the input file (Supporting Information) for the Rice−Ramsperger−Kassel−Marcus Master Equation (RRKM-ME) calculations of temperature- and pressure-dependent reaction rate constants as implemented in the MESS package.[62,63] For the atomic hydrogen loss channels, which feature relatively low reverse barriers, the rate constants were computed employing variational transition state theory (VTST). Here, intrinsic reaction coordinate (IRC) calculations were run using internal coordinates to map out the minimal energy reaction path (MEP) at the ωB97X-D/6-311G(d,p) level, and the MEP potential was uniformly scaled to match the ωB97X-D/6-311G(d,p) barrier height to the high-level FNO−CCSD(T)/CBS value. The collisional energy transfer in ME was treated within the "exponential down" model,[64] where the temperature dependence of the range parameter α for the deactivating wing of the energy transfer function was expressed as $\alpha(T) = \alpha_{300}(T/300\ \mathrm{K})^n$, with n = 0.62 and α_{300} = 424 cm^{-1} derived earlier from classical trajectory calculations.[21,65] These values, along with the Lennard-Jones parameters ε = 390 cm^{-1} and σ = 4.46 Å, were adopted from our earlier studies of the reaction kinetics involving the $C_{10}H_9$ PES.[21,31,66] The MESS input file is attached in the Supporting Information as mess.inp. The InChIs of all species are available in Table S3. Arrhenius fits of the rate constants of the main reaction pathways are reported in the PLOG format and are attached as DETAILED-CKI. To allow for a continuous temperature range of the fitting at all pressures (i.e., overcoming the partial temperature and pressure ranges of thermochemical stabilization for many of the wells), the MESS WellExtension option coupled with WellExtensionCaps properly selected was used. In the fitting procedure, rate constants showing negative values, oscillating behavior, and too low fitting quality were deleted. To reduce the final set of rate constants, reaction paths contributing to less than 10^{-6} to the product distribution were also ignored. A higher fraction would lead to incorrect representation of some of the equilibrated products (e.g., naphthalene and fulvalene with the corresponding wells). Overall, the final set of rate constants consists of 36 species and 453 (irreversible) reactions.

4. KINETIC MODELING

Kinetic modeling was performed to assess the relevance of the reaction pathways investigated for $C_7H_5^{\cdot} + C_3H_4$ at both the experimental conditions of the flow reactor and at different combustion conditions where PAH growth from fulvenallenyl was highlighted to be relevant. A small kinetic model was assembled for the kinetic simulations of the flow reactor experiments, which included: the reactions on the PESs of $C_7H_5^{\cdot} + C_3H_4$ from this work (both the addition and the abstraction reactions); the H-abstractions by Cl atoms from C_3H_4,[67] the hydrogen atom-assisted isomerization of azulene to naphthalene via the spiran mechanism (not treated in this work),[27] and the reactions on the $C_7H_5^{\cdot} + C_3H_3^{\cdot}$ PES recently presented by Li et al.[44] Additionally, we considered the main reactions of Cl/HCl mechanism from the recent kinetic model of Pelucchi et al.[68] and the main decomposition pathways of fulvenallene and fulvenallenyl derived from literature theoretical calculations and kinetic model estimates.[40] The kinetics of $C_7H_5^{\cdot}$ self-recombination to form three-membered ring aromatic species was also estimated from that of the analogous reaction of the propargyl radical.[4,69] The kinetics of the complex $C_7H_5^{\cdot} + C_3H_4/C_3H_3^{\cdot}$ PESs was simplified using MEL, an open-source master equation-based lumping tool.[70] Lumped groups of species for the $C_7H_5^{\cdot} + C_3H_3^{\cdot}$ PES are reported in Table S2, while those for $C_7H_5^{\cdot} + C_3H_4$ are reported in Table S3. The Arrhenius fits for the set of lumped rate constants of $C_7H_5^{\cdot} + C_3H_4$ PES are attached as LUMPED-CKI, while the temperature and pressure-dependent composition of the pseudospecies are reported in a separate folder in the Supporting Information. Similar criteria to those employed in the fitting of detailed rate constants were adopted in the postprocessing of MESS output. Overall, the final set of lumped rate constants consists of 20 species and 213 reactions. Poorer performances of the lumped mechanism with respect to detailed rate constant fitting are obtained at 0.01 atm.

The microreactor was simulated as a simple plug flow reactor imposing temperature, pressure, and velocity profiles previously derived from computational fluid dynamics simulations of analogous systems.[22,71] In particular, previously derived profiles were shifted so as to match the estimated plateau temperature of 1000 K and the estimated inlet flow rate of 48 sccm, which corresponds to an inlet gas velocity of ∼21 m/s and a total residence time of under 1 ms. The simulation software used is OpenSMOKE++.[72] Despite the somewhat large uncertainty in the pressure and velocity profiles imposed, we verified that the macroscopic quantities of interest at the exit of the reactor show little sensitivity to such uncertainty, as exemplified in the results. Additional details on the temperature, pressure, and velocity profiles adopted are found in the Supporting Information (Figure S11). The uncertainty in the estimated temperature profile only affects how rapidly the product distribution at the reactor exit is

https://doi.org/10.1021/acs.jpca.4c02386
J. Phys. Chem. A 2024, 128, 5707−5720

reached since the outlet product branching fractions are essentially governed by the value of the temperature plateau. As a result, the small estimated experimental uncertainty of the temperature plateau of ±10 K leads to negligible variations in the estimated product distribution at the reactor outlet. At the reactor inlet, the $C_7H_5Cl_3$ precursor was assumed to have already dissociated. Since the detailed decomposition mechanism was not accounted for in the kinetic model, we verified that the aromatics product distribution is unvaried, assuming either $C_7H_5^{\cdot}$ + 3Cl$^{\cdot}$ or $C_7H_5^{\cdot}$ + Cl$^{\cdot}$ + Cl_2 as dissociation products of the precursor (i.e., reactor inlets; see Table S5). Finally, while we believe that direct HCl elimination from the precursor is inactive as it was not detected experimentally, we verified with kinetic simulations that the presence of HCl at the reactor inlet does not affect the product distribution because HCl does not react according to any active pathway in the chlorine submechanism.

To better assess the impact of the investigated reaction pathway and its competition with the radical growth pathway (i.e., fulvenallenyl recombination with propargyl), we also performed kinetic simulations at different operating conditions. In particular, we considered the high-pressure shock tube experiments of Sun et al.[50] for the copyrolysis of toluene and methylacetylene, where their kinetic model highlighted the relevance of the $C_7H_5^{\cdot}$ + $C_3H_3^{\cdot}$ reaction to naphthalene formation. In this case, we updated the kinetic model of Sun et al. with the lumped rate constants for both $C_7H_5^{\cdot}$ + $C_3H_3^{\cdot}$ and $C_7H_5^{\cdot}$ + C_3H_4 PESs. It is noted that in the starting model, these reaction pathways were approximated by analogy with propargyl radical reactions and produced only 1-methylene-1*H*-indene ($C_9H_6CH_2$ in the model) and naphthalene, hence all the new species of the lumped sets of rate constants were added.

5. EXPERIMENTAL RESULTS

Representative mass spectra recorded at a photon energy of 9.00 eV are displayed in Figure 1c/d. Control experiments of helium-seeded trichloromethylbenzene ($C_7H_5Cl_3$) were also conducted at 373 ± 10 K and 998 ± 10 K (Figure 1a,b), respectively. At 373 ± 10 K, only ion counts of the trichloromethylbenzene precursor (194 amu., $C_7H_5{}^{35}Cl_3^+$; 195 amu., $^{13}CC_6H_5{}^{35}Cl_3^+$; 196 amu., $C_7H_5{}^{35}Cl_2{}^{37}Cl^+$; 197 amu., $^{13}CC_6H_5{}^{35}Cl_2{}^{37}Cl^+$; 198 amu., $C_7H_5{}^{35}Cl^{37}Cl_2^+$; 199 amu., $^{13}CC_6H_5{}^{35}Cl^{37}Cl_2^+$; and 200 amu., $C_7H_5{}^{37}Cl_3^+$) are detectable (Figure 1a). With the rise of the experimental temperature to 998 ± 10 K, the stepwise elimination of chlorine (Cl) atoms from the trichloromethylbenzene ($C_7H_5Cl_3$) precursor occurs (Figure 1b, green; Figures S1−S4), and new ion counts emerge at m/z = 174 ($C_{14}H_6^+$), 176 ($C_{14}H_8^+$), and 178 ($C_{14}H_{10}^+$) (Figure S5). Concerning HCl elimination from the precursor, it can be seen that there is no signal collected at m/z = 158 (corresponding to $C_7H_4{}^{35}Cl_2$), which means HCl elimination directly from $C_7H_5{}^{35}Cl_3$ molecule does not occur. The ion count at m/z = 123 (corresponding to $C_7H_4{}^{35}Cl$) was collected, and it might originate from HCl elimination from $C_7H_5{}^{35}Cl_2$. However, $C_7H_4{}^{35}Cl$ cannot lead to the formation of C_7H_5. This means that even if the HCl elimination mechanism exists in the decomposition process of trichlorobenzene, it does not affect the formation of the target fulvenallenyl radical. Once methylacetylene (CH_3CCH) or allene (H_2CCCH_2) is added to the reaction systems, the ion count of interest emerges at m/z = 128 (Figure 1c,d, red); this peak is absent in the reference experiments (Figure 1a,b). Accounting for the

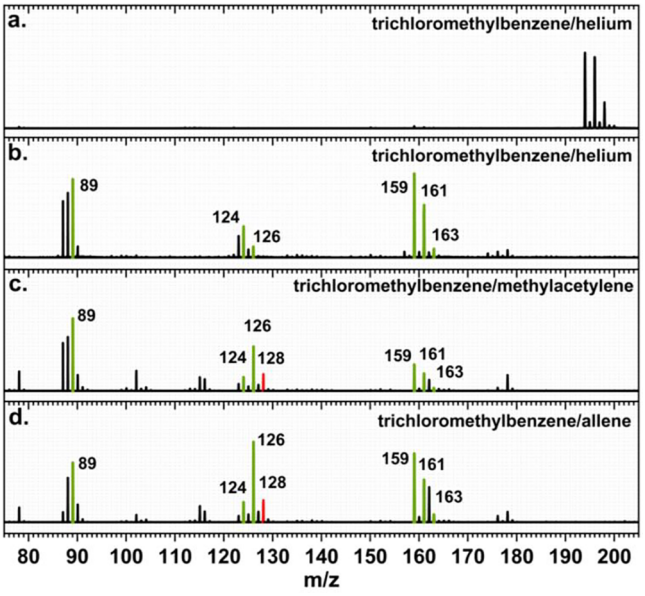

Figure 1. Mass spectra recorded at a photoionization energy of 9.00 eV. (a) Trichloromethylbenzene-helium system at 373 ± 10 K; (b) trichloromethylbenzene-helium system at 998 ± 10 K; (c) trichloromethylbenzene-methylacetylene system at 998 ± 10 K; (d) trichloromethylbenzene-allene system at 998 ± 10 K. The interested ion counts at m/z = 128 are highlighted in red.

molecular weight of reactants ($C_7H_5^{\cdot}$, 89 amu; C_3H_4, 40 amu) and product (s) ($C_{10}H_8$, 128 amu), the formation of molecules with the formula $C_{10}H_8$ can be linked to the reaction of fulvenallenyl with methylacetylene or allene accompanied by the loss of atomic hydrogen. In addition to the signal at m/z = 128, ion counts originating from byproducts also emerge at m/z = 78 ($C_6H_6^+$), 102 ($C_8H_6^+$), 115 ($C_9H_7^+$), and 116 ($C_9H_8^+$) (Figures S5−S7).

The detailed analysis of the corresponding PIE curves of the ions at m/z = 128 ($C_{10}H_8^+$) and 129 ($^{13}CC_9H_8^+$) allows for an *isomer selective* identification of the molecules at the relevant masses. The experimental PIE curves of m/z = 128 (Figure 2a,c) can be nicely reproduced by a linear combination of the reference curves of two $C_{10}H_8$ isomers: azulene (**1**)[44] and naphthalene (**2**).[73] The onset value, 7.45 ± 0.05 eV, of the ion counts at m/z = 128 practically coincides with the adiabatic ionization energy (IE) of azulene of 7.42 ± 0.02 eV.[74] Contribution from naphthalene, which has an adiabatic ionization energy (IE) of 8.14 ± 0.05 eV,[75] to the experimental PIE curves of m/z = 128 becomes critical starting from 8.15 ± 0.05 eV. The excellent match of the experimentally recorded PIEs at m/z = 128 provides a persuasive identification of azulene and naphthalene with branching ratios of the ion counts of 6.0 ± 0.6:94.0 ± 9.4 and 9.4 ± 0.9:90.6 ± 9.1% at 8.40 eV in fulvenallenyl-methylacetylene and fulvenallenyl-allene systems, respectively. Accounting for the photoionization cross sections of azulene and naphthalene of 10.79 ± 1.29[44] and 5.23 ± 0.63[44] Mb (Mega barn, 1 barn = 10^{-24} cm^2), respectively, at 8.40 eV, branching ratios of 9.4 ± 3.8:90.6 ± 3.8% and 4.8 ± 3.4:95.2 ± 3.4% are determined in fulvenallenyl-methylacetylene and fulvenallenyl-allene systems, respectively. The identification of naphthalene and azulene can be further confirmed through the analysis of the PIE curves at m/z = 129 ($^{13}CC_9H_8^+$) (Figure 2b,d). Note that the experimental PIE curves of the fulvenallenyl radical ($C_7H_5^{\cdot}$)

https://doi.org/10.1021/acs.jpca.4c02386
J. Phys. Chem. A 2024, 128, 5707−5720

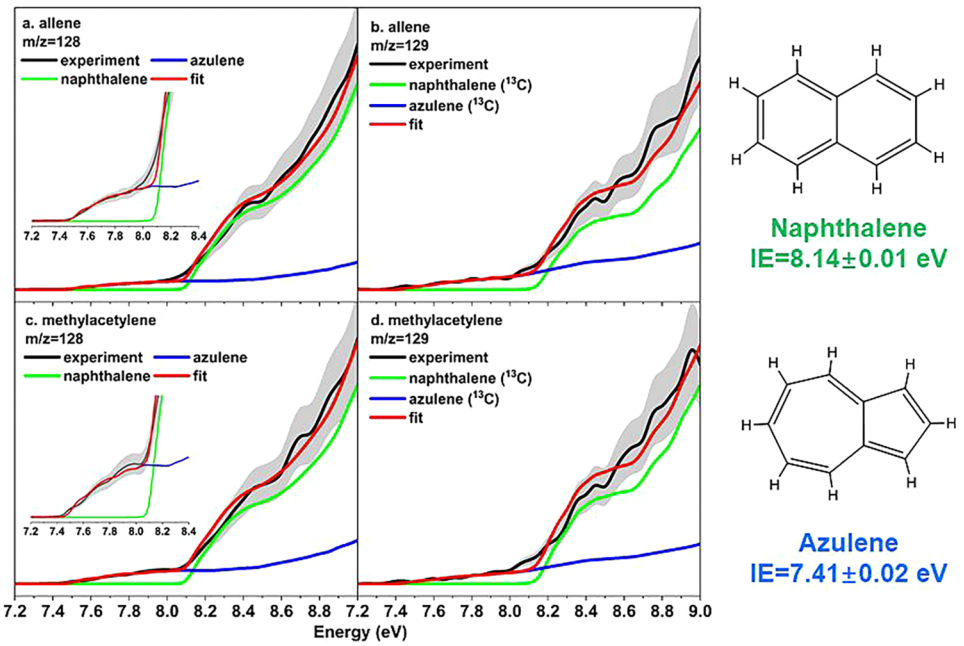

Figure 2. Experimental and reference PIE curves of m/z = 128 and 129. The black line refers to the experimental data. The overall error bars consist of three parts: ±10% based on the accuracy of the photodiode, ±5% considering the injection stability, and a 1σ error of the PIE curve averaged over the individual scans. The color-coded lines refer to the reference PIE curves of azulene (blue) and naphthalene (green) isomers. The red line shows the overall fit via the linear combination of the reference curves.

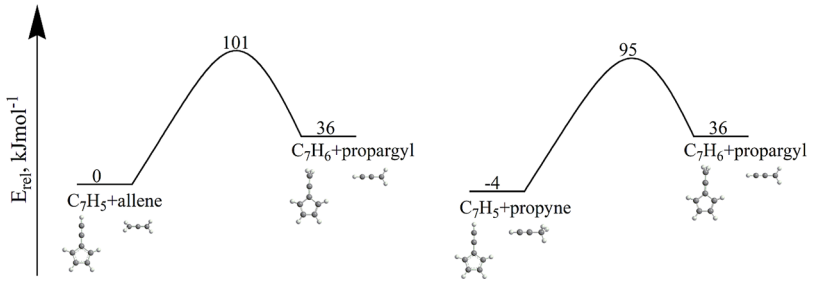

Figure 3. Potential energy diagrams for the direct H-abstraction channels in the $C_7H_5^{\cdot}$ + C_3H_4 reactions. All relative energies given in kJ mol^{-1} are calculated at the FNO−CCSD(T)/CBS//ωB97X-D/6-311G(d,p) + ZPE(ωB97X-D/6-311G(d,p)) level of theory.

(Figure S8a,b) generated from trichloromethylbenzene thermo-decomposition are also provided, along with a reference PIE curve of fulvenallenyl generated from phthalide pyrolysis,[76] which verifies an efficient precursor, trichloromethylbenzene, for fulvenallenyl preparation.

6. COMPUTATIONAL RESULTS

6.1. Potential Energy Surfaces. *6.1.1. Fulvenallenyl Plus Allene.* According to the calculated PES, the reactions of fulvenallenyl radical ($C_7H_5^{\cdot}$) with allene and methylacetylene (C_3H_4) can proceed via either hydrogen atom abstraction or addition-isomerization-H-elimination pathways. Direct hydrogen atom abstraction leads to fulvenallene (C_7H_6) plus propargyl ($C_3H_3^{\cdot}$) with both reactions predicted to be endoergic by 36 (allene) and 40 (methylacetylene) kJ mol^{-1} proceeding over barriers of 101 and 99 kJ mol^{-1}, respectively (Figure 3). In the case of methylacetylene, the hydrogen atom abstraction occurs from the methyl group since the C−H bond in the CH_3 moiety of methylacetylene is much weaker than its acetylenic C−H bond. Indeed, the 1-propynyl radical ($^{\cdot}CCCH_3$) is 175 kJ mol^{-1} less stable than the propargyl radical ($HCCCH_2^{\cdot}$),[77] and hence we neglected the acetylenic hydrogen abstraction pathway in the present study.

In detail, the PES for allene addition to fulvenallenyl is illustrated in Figure 4, with a number of less favorable reaction channels featured in Figure S9 in the Supporting Information. As the radical position in fulvenallenyl is delocalized over the entire molecule,[44] we considered the additions to the terminal carbon in the side chain ($C_7H_5^{\cdot}$ + H_2CCCH_2 → **i2**) and to the five-membered ring's C atoms in the *ortho* and *ipso* positions with respect to the side chain ($C_7H_5^{\cdot}$ + H_2CCCH_2 → **i1**/**i3**); we did not consider the *meta* addition here as it is not conducive for the formation of a second ring, with two side chains being too far from one another in the addition complex. The **i1** and **i2** $C_{10}H_9$ entrance complexes are only slightly stabilized with respect to the reactants, by 15 and 24 kJ mol^{-1}, respectively, whereas the *ipso* addition complex **i3** lies 14 kJ mol^{-1} above the reactants. The allene addition steps feature sizable barriers of 59, 69, and 68 kJ mol^{-1} to produce **i1**, **i2**, and **i3**, respectively. From **i1**−**i3**, the reaction can proceed either by immediate but highly endothermic hydrogen atom losses from various positions, among which the most favorable ones lead to the formation of **p5** and **p6**, or through a sophisticated maze of pathways eventually leading to the

https://doi.org/10.1021/acs.jpca.4c02386
J. Phys. Chem. A 2024, 128, 5707−5720

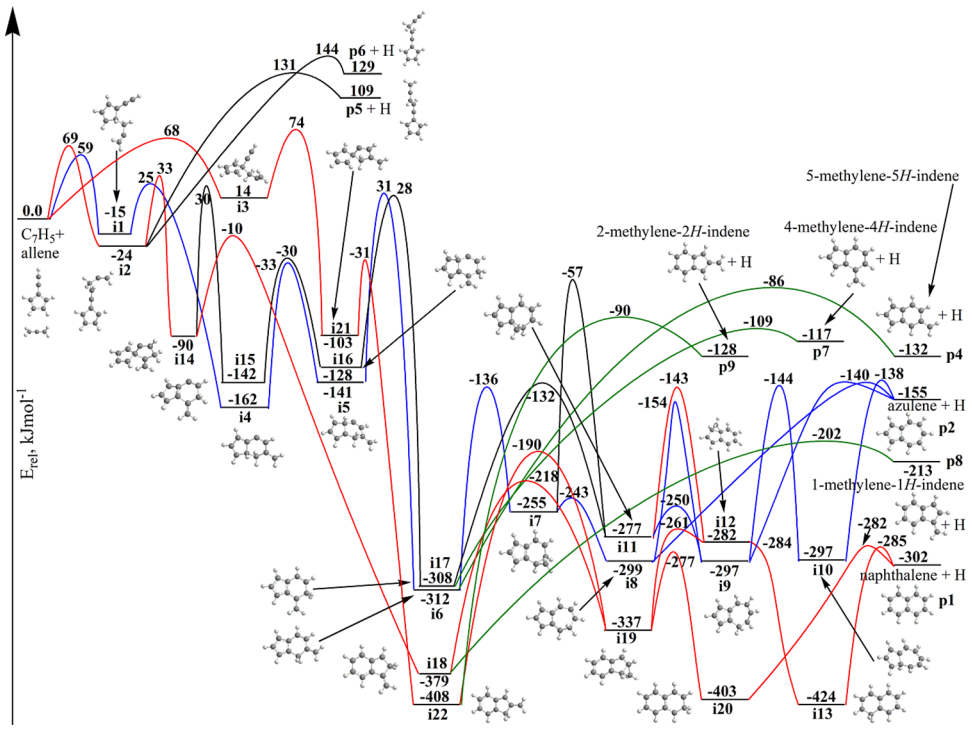

Figure 4. Potential energy diagram for the addition(-isomerization)-elimination channels in the $C_7H_5^{\cdot}$ + allene reaction. All relative energies given in kJ mol^{-1} are calculated at the FNO−CCSD(T)/CBS//ωB97X-D/6-311G(d,p) + ZPE(ωB97X-D/6-311G(d,p)) level of theory. Red, blue, and green curves show the most favorable pathways leading to naphthalene, azulene, and methyleneindenes, respectively.

formation of more favorable bicyclic $C_{10}H_8$ isomers, including naphthalene **p1**, azulene **p2**, and various methyleneindenes **p4**, **p7**−**p9**. In particular, the *ortho* addition complex **i1** can undergo a six-membered ring closure to **i4** via a transition state (TS) residing 25 kJ mol^{-1} above the reactants. Next, **i4** is subjected to two consecutive 1,2-H shifts in the newly formed six-membered ring, **i4** → **i5** → **i6**, with the highest in energy TS for the second step lying 30 kJ mol^{-1} higher in energy than $C_7H_5^{\cdot}$ + allene. The intermediate **i6** resides in a deep potential (−312 kJ mol^{-1}) and can further undergo an H loss producing 5-methylene-5*H*-indene (−132 kJ mol^{-1}) or feature another 1,2-H shift **i6** → **i7** followed by the insertion of the methylene group into the six-membered ring **i7** → **i8** and an H loss from **i8** producing azulene (−155 kJ mol^{-1}). The H atom elimination can occur directly from **i8**, or be preceded by one or two H migrations around the seven-membered ring, **i8** → (**i9** → (**i10** →)) **p2** + H, where the direct **i8** → **p2** + H is most favorable kinetically. The least favorable route from **i7** is a methylene walk (CH_2 group migration) to **i11**, which can be followed by either facile CH_2 insertion into the ring, **i11** → **i9**, and an H loss producing azulene from **i9**, or by another methylene walk step, **i11** → **i12**, with the CH_2 group moving onto the five-membered ring, occurring via a higher barrier. The **i12** intermediate can only be metastable as the barrier for the CH_2 insertion into the five-membered ring disappears when the energies of **i12** and TS (**i12** → **i13**) are refined at the high level of theory. **i13**, the 1-naphthalenyl radical, loses a hydrogen from CH_2 forming the most thermodynamically favorable product naphthalene (−302 kJ mol^{-1}).

A more competitive route to naphthalene initiates from the tail addition complex **i2**. Here, a five-membered ring closure of the long side chain leads to a spiro structure **i14** having two cyclopenta rings in perpendicular planes via a TS located 33 kJ mol^{-1} above the reactants. Next, one of the rings pivots into the plane of the other ring and expands to a six-membered ring, producing a low-energy isomer **i18** (−379 kJ mol^{-1}) via a relatively small barrier (TS at −10 kJ mol^{-1}). The intermediate **i18** can either lose an H atom forming 1-methylene-1*H*-indene (**p8**, −213 kJ mol^{-1}) or undergo a three-step isomerization and decomposition to naphthalene, **i18** → **i19** → **i20** → **p1** + H, involving H shift, CH_2 insertion into the five-membered ring, and H elimination. Along this path, the immediate precursor of naphthalene is 2-naphthalenyl radical **i20**. The reaction can also proceed via 1-naphthalenyl radical **i13** if **i19** undergoes a methylene walk step prior to the CH_2 ring insertion, **i19** → **i12** → **i13** → **p1** + H. The channel from **i14** to azulene is less preferable than those leading to naphthalene, as the initial five-membered ring rotation and expansion step **i14** → **i15** features a higher barrier, 40 kJ mol^{-1} higher than that for **i14** → **i18**. Then, two 1,2-H shifts in **i15** lead to **i17** via **i16**, and **i17** can either dissociate to 4-methylene-4*H*-indene (**p7**, −117 kJ mol^{-1}) or proceed to **i11** via one more H migration. The pathways from **i11** to azulene and naphthalene, **i11** → **i9** → **p2** + H and **i11** → **i12** → **i13** → **p1** + H, are competitive, with the bottleneck TSs positioned at −140 and 143 kJ mol^{-1}, respectively. The *ipso* addition complex **i3** also favors the formation of naphthalene. Here, the reaction proceeds via a five-membered closure involving two side chains linked to the same C atom in the ring, producing the other spiro isomer **i21**. The latter rearranges to **i22** (−408 kJ mol^{-1}), which can in turn dissociate to 2-methylene-2*H*-indene (**p9**, −128 kJ mol^{-1}) or merge onto the naphthalene producing pathway via the H migration step **i22** → **i19**.

Interestingly, the group of the $C_{10}H_9$ intermediates **i7**−**i12**, **i19**, and **i20** have been described earlier as a part of the "methylene walk" pathway for the H-assisted azulene-naphthalene isomerization.[25] It is noteworthy that a pathway to fulvalene, **i2** → **i35** → (**i40** →) **p3** + H (Figure S9) is less

https://doi.org/10.1021/acs.jpca.4c02386
J. Phys. Chem. A 2024, 128, 5707−5720

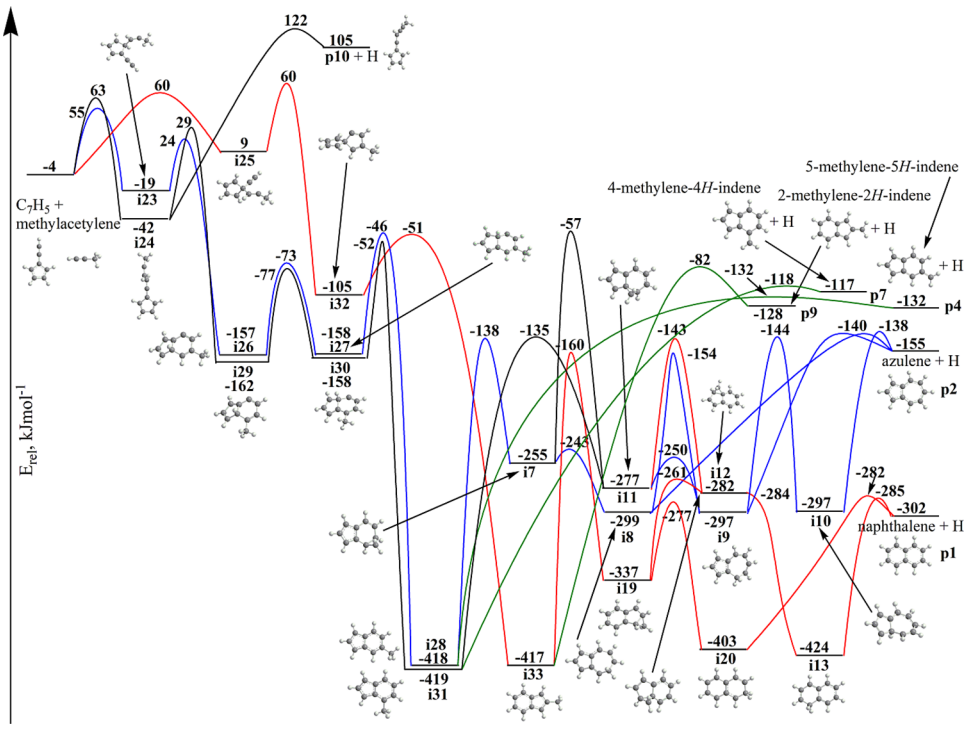

Figure 5. Potential energy diagram for the addition(-isomerization)-elimination channels in the $C_7H_5^{\cdot}$ + methylacetylene reaction. All relative energies given in kJ mol^{-1} are calculated at the FNO−CCSD(T)/CBS//ωB97X-D/6-311G(d,p) + ZPE(ωB97X-D/6-311G(d,p)) level of theory. Red, blue, and green curves show the most favorable pathways leading to naphthalene, azulene, and methyleneindenes, respectively.

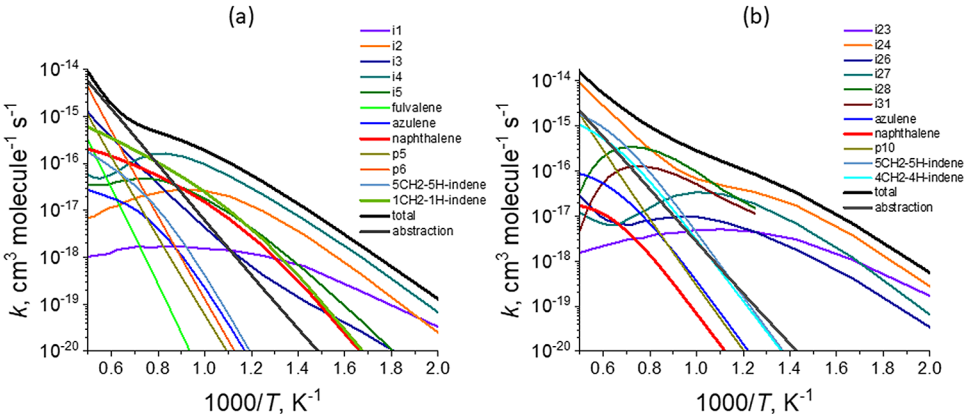

Figure 6. RRKM-ME rate constants calculated for 1 atm (independent of pressure for the direct H-abstraction channels) for (a) $C_7H_5^{\cdot}$ + allene; (b) $C_7H_5^{\cdot}$ + methylacetylene.

competitive because the barrier for the five-membered ring closure **i2** → **i35** is positioned as high as 174 kJ mol^{-1} above the reactants. The **i40** and **i35** intermediates are easily accessed by the cyclopentadienyl self-recombination $C_5H_5^{\cdot}$ + $C_5H_5^{\cdot}$ followed by an H atom loss.[25,26] Thus, the two reactions, $C_7H_5^{\cdot}$ + C_3H_4 and $C_5H_5^{\cdot}$ + $C_5H_5^{\cdot}$ → $C_{10}H_{10}$ → $C_{10}H_9^{\cdot}$ (n*H*-fulvalenyl radicals) + H initiate from rather distinct regions of the vast $C_{10}H_9$ PES. Alternatively, isomerization on the $C_{10}H_{10}$ surface following the $C_5H_5^{\cdot}$ recombination and subsequent H losses can lead to n*H*-azulenyl radicals,[26] which are also found among the intermediates in the present study (**i8**−**i10**).

6.1.2. Fulvenallenyl Plus Methylacetylene. The pattern of the $C_7H_5^{\cdot}$ plus methylacetylene PES (Figures 5 and S10 in the Supporting Information) is generally similar to that described above (Section 6.1.1). In this case, *ortho*, tail, and *ipso* additions of methylacetylene to the fulvenallenyl radical by the acetylenic end form intermediates **i23**, **i24**, and **i25**, 15 and 38 kJ mol^{-1} below and 13 kJ mol^{-1} above the reactants via barriers of 59, 67, and 64 kJ mol^{-1}, respectively. The most favorable among endothermic hydrogen atom losses produces **p10** from **i24**, with the product and exit barrier lying 109 and 126 kJ mol^{-1} higher in energy than the separated reactants, respectively. The pathway initiating from the *ortho* adduct **i23** favors the formation of azulene (**p2**) along with 5-methylene-5*H*-indene (**p4**), where **i23** first undergoes a six-membered ring closure to **i26** followed by two 1,2-H shifts leading to a deep potential well at **i28** (−414 kJ mol^{-1} relative to $C_7H_5^{\cdot}$ + methylacetylene) via **i27**. Next, **i28** either dissociates to **p4** + H or features another H migration from the methyl group to the neighboring C atom in the ring forming **i7**. As discussed in Section 6.1.1, **i7** can produce azulene via the **i8** → (**i9** → (**i10** →)) **p2** + H route. The tail addition to **i24** is also followed by

https://doi.org/10.1021/acs.jpca.4c02386
J. Phys. Chem. A 2024, 128, 5707−5720

a six-membered ring closure to **i29** and two H migrations leading to **i31**. This channel is very similar to **i23** → **i26** → **i27** → **i28**, and structures and energies of **i31** and **i28** differ merely by the position of the CH_3 group attached to the six-membered ring. The low-lying intermediate **i31** can lose a hydrogen atom forming 4-methylene-4*H*-indene **p7**. Otherwise, H migration from the methyl group leads to **i11** which can dissociate to either azulene or naphthalene via the two competitive channels, **i11** → **i9** → (**i10** →) **p2** + H and **i11** → **i12** → **i13** → **p1** + H, respectively. The reaction channel starting from the *ipso* adduct **i25** preferably leads to naphthalene along with 2-methylene-2*H*-indene (**p9**). **i25** first features a five-membered ring closure to form a spiro isomer **i32**, which then proceeds by a ring rotation and expansion to a deep local minimum **i33** (−413 kJ mol^{-1}). The latter can eliminate an H atom to form **p9** or rearrange by H migration to **i19** and to eventually decompose to naphthalene via the **i19** → **i20** → **p1** + H or **i19** → **i12** → **i13** → **p1** + H or routes.

6.2. Reaction Kinetics and Preferential Products. The total and individual channel rate constants for the $C_7H_5^{\cdot}$ + allene/methylacetylene reactions at 1 atm are illustrated in Figure 6a,b. One can see that the reactions are generally slow because of the relatively high entrance barriers and the competitiveness of the reverse decomposition of the initial adducts with the forward isomerization-decomposition channels. For the reaction with allene, the total addition rate constant grows from 1.3×10^{-19} to 8.9×10^{-15} cm^3 mol^{-1} s^{-1} in the 500−2000 K range and remains higher than the H-abstraction rate constant $C_7H_5^{\cdot}$ + allene → C_7H_6 + propargyl, 1.9×10^{-23} to 5.5×10^{-15} cm^3 mol^{-1} s^{-1}, in the entire considered temperature interval. At low temperatures, the addition reaction forms mostly the collisionally stabilized adducts **i1**, **i2**, and the intermediate **i4**, which is easily produced from **i1**. The overall yield of these three intermediates eventually reduces from ∼97% at 500 K to 65 and 12% at 1000 and 1500 K, respectively. Interestingly, the calculated branching ratio of the collisionally stabilized **i3**, which is insignificant at low temperatures, grows to ∼19% at 1600−1700 K and then slightly decreases at higher temperatures. Among the bimolecular H elimination products, 1-methylene-1*H*-indene and naphthalene are preferred up to high temperatures (1700 K and above), where the formation of **p6** becomes favorable as the rate constant leading to its formation increases more rapidly because of entropic contributions. The relative yields of 1-methylene-1*H*-indene and naphthalene, 26.7 and 12.3%, are maximum at 1400 K. Azulene and fulvalene are predicted to be minor products, whereas the branching ratio of the latter grows with temperature and even exceeds that of naphthalene at 2000 K, 3.5 vs 2.3%. The computed rate constants for the formation of 1-methylene-1*H*-indene and naphthalene at the typical combustion temperature of 1500 K are only 2.3×10^{-16} and 1.1×10^{-16} cm^3 mol^{-1} s^{-1}, indicating that the $C_7H_5^{\cdot}$ + allene reaction is unlikely to give a significant contribution to the naphthalene production in combustion flames. At the temperature of the present experiment in the microreactor, 1000 K, the rate constants for the formation of the observed products, naphthalene and azulene, are as low as 1.5×10^{-17} and 2.3×10^{-19} cm^3 mol^{-1} s^{-1}. The pressure dependence of the rate constants for the reaction channels leading to the preferable bimolecular products is found to be insignificant at temperatures relevant to combustion. For instance, for 1-methylene-1*H*-indene and naphthalene, the rate constants at 1500 K vary in the 2.4×10^{-16}−2.2×10^{-16} and 1.1×10^{-16}−9.5×10^{-17} cm^3 mol^{-1} s^{-1} ranges at p = 0.01−10 atm.

The $C_7H_5^{\cdot}$ + methylacetylene reaction is also predicted to be slow, 5.6×10^{-19}−1.6×10^{-14} cm^3 mol^{-1} s^{-1} at 1 atm and 500−2000 K for the addition channel vs 1.0×10^{-23}−2.1×10^{-15} cm^3 mol^{-1} s^{-1} for the direct H-abstraction channel giving C_7H_6 + propargyl. For the addition reaction, the collisional stabilization of the tail adduct **i24** is favored in the entire considered temperature range, with **i23**, **i26**, **i27**, and deep potential wells **i28** and **i31** also giving significant contributions at varying temperatures. 5-Methylene-5*H*-indene and 4-methylene-4*H*-indene produced by H losses from **i28** and **i31**, along with **p10** formed directly from the initial adduct **i24**, represent the preferred bimolecular products, with their branching ratios being, respectively, e.g., 17, 10, and 3%, at 1500 K. Here, azulene (up to 1.1%) and naphthalene (up to 0.2%) are only trace products, with channel-specific rate constants of 3.1×10^{-17} and 6.6×10^{-18} cm^3 mol^{-1} s^{-1} at 1500 K and 3.6×10^{-19} and 6.8×10^{-20} cm^3 mol^{-1} s^{-1} at 1000 K. Finally, it is noted that the total high-pressure limit rate constants computed are significantly slower than the estimates currently adopted in kinetic models (e.g., Sun et al.[50]), i.e., by about a factor of 5 at 1500 K up to more than 1 order of magnitude at lower temperatures. This aspect highlights (1) the need to update literature combustion models with the present results and (2) the relevance of the investigated reaction pathways will likely decrease compared to the current model predictions.

Considering the slow total reaction rate and the minor formation of bimolecular products, and most notably of naphthalene and azulene, identified in the experiment as main products, we conclude that the $C_7H_5^{\cdot}$ + C_3H_4 reaction cannot account for the experimental observations. Instead, it is possible that the formation of naphthalene and azulene may rather stem from the faster $C_7H_5^{\cdot}$ + $C_3H_3^{\cdot}$ radical−radical reaction, which we investigated in the earlier study.[44] The main source of the propargyl radical in the present experiment could likely be the direct hydrogen abstraction from allene and methylacetylene by chlorine atoms produced by the decomposition of the trichloromethylbenzene precursor. In order to verify this hypothesis, we carried out macroscopic kinetic modeling of the physicochemical processes in the reactor.

6.3. Kinetic Simulations. Figure 7 shows the mole fraction profiles of the main species as a function of the residence time in the microreactor for the $C_7H_5^{\cdot}$ + C_3H_4-P and C_3H_4-A systems. The simulated species profiles reveal that the early consumption of C_3H_4 is mirrored by the formation of $C_3H_3^{\cdot}$ (see bottom of Figure 7). In fact, the flux analysis confirms that C_3H_4 is almost entirely consumed from H-abstractions by Cl atoms. Instead, the small decrease in Cl mole fraction observed at longer residence times is associated with its self-recombination to Cl_2. The faster consumption of C_3H_4-A with respect to C_3H_4−P is due to the faster rate constant of the corresponding H-abstraction reaction. Hence, it is reasonable to conclude that the addition of C_3H_4 to the fulvenallenyl radical is not competitive with its secondary reactivity in the temperature range of the experiment. Such behavior persists even in excess of C_3H_4, namely when it is assumed that the $C_7H_5^{\cdot}$ precursor dissociates to $C_7H_5^{\cdot}$ + Cl_2 + $Cl^{\cdot}$. The corresponding simulation profiles are reported in the Supporting Information.

https://doi.org/10.1021/acs.jpca.4c02386
J. Phys. Chem. A 2024, 128, 5707−5720

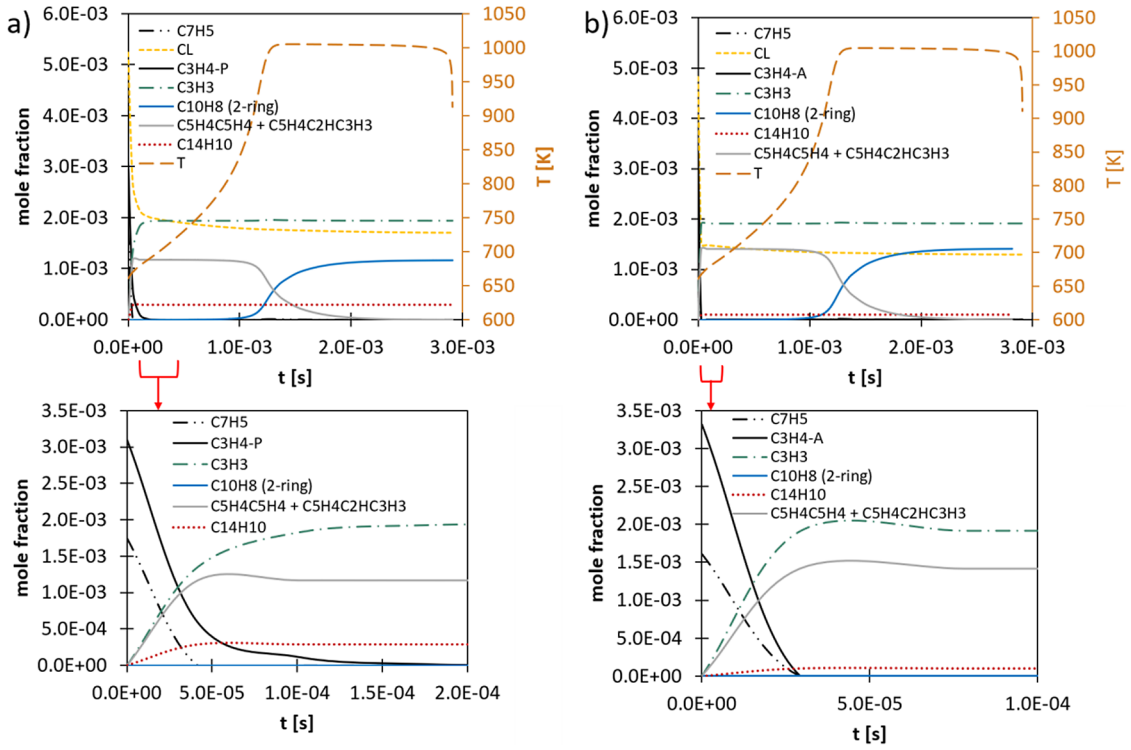

Figure 7. Simulated profiles of the main species at the reactor outlet for (a) the $C_7H_5^{\cdot}$/Cl/C_3H_4−P system and (b) for the $C_7H_5^{\cdot}$/Cl/C_3H_4-A system using the estimated temperature profile. Additional simulation results are found in the Supporting Information. The bottom of each figure zooms in on the first instants of the reactor, where C_3H_4 is converted.

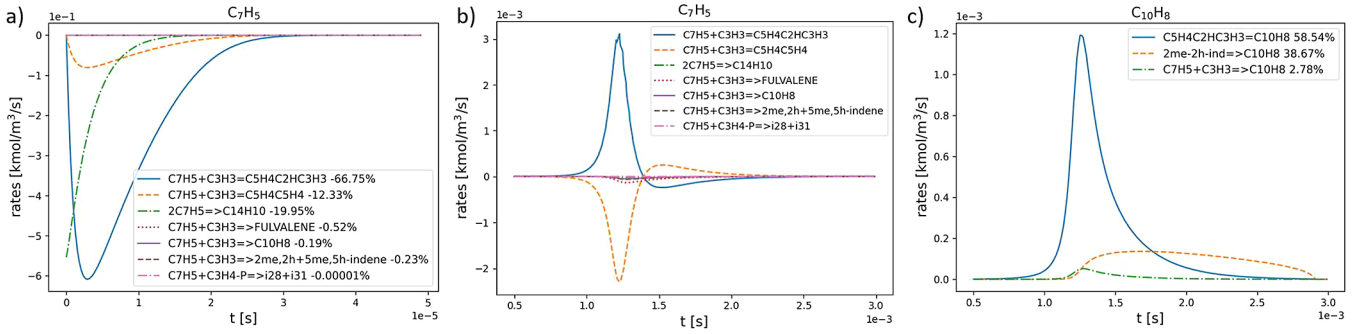

Figure 8. Reaction rates relevant in the consumption and formation of fulvenallenyl ($C_7H_5^{\cdot}$) and naphthalene ($C_{10}H_8$) in the simulated microtubular reactor for the $C_7H_5^{\cdot}$/Cl/C_3H_4−P system (see Figure 7a). (a) Main consumption pathways of fulvenallenyl in the first part of the reactor, while (b,c) report reaction rates in the region of the two-ring PAH formation. The % indicates the relative contribution of each reaction to the production/consumption of each species integrated over the residence time in the reactor.

Figure 8a reports the reaction rates mostly responsible for fulvenallenyl consumption in the first instants of the reactor for the $C_7H_5^{\cdot}$ + C_3H_4−P system. $C_7H_5^{\cdot}$ is first consumed via self-recombination to $C_{14}H_{10}$, which was also detected in the experimental measurements. Then, as soon as $C_3H_3^{\cdot}$ radicals are generated via H-abstraction reactions, they recombine with $C_7H_5^{\cdot}$ and form $C_{10}H_8$ isomers, whose onset is right after that of propargyl radicals. In fact, the total rate constant of $C_7H_5^{\cdot}$ + $C_3H_3^{\cdot}$ is about 6×10^{-11} cm^3 mol^{-1} s^{-1} at 1000 K and 0.1 atm, while the rate constants for $C_7H_5^{\cdot}$ + C_3H_4 are more than 5 orders of magnitude smaller. This is reflected by the relative contribution of these pathways to fulvenallenyl consumption, as highlighted in Figure 8a: the radical pathway accounts for about 80% of fulvenallenyl consumption, while the most relevant reaction of the molecular pathway (forming **i28** + **i31**) plays a negligible role (0.00001% of the reactant consumption). Hence, the generation of $C_3H_3^{\cdot}$ radicals via H-abstraction reactions indirectly controls fulvenallenyl consumption, which also explains the faster fulvenallenyl decay in the $C_7H_5^{\cdot}$/C_3H_4-A system. Overall, it is concluded that the products observed in the microtubular reactor experiments are formed from the fast $C_7H_5^{\cdot}$ + $C_3H_3^{\cdot}$ and $C_7H_5^{\cdot}$ + $C_7H_5^{\cdot}$ recombination reactions, as also confirmed by the similarity of the product distribution measured in the previously investigated $C_7H_5^{\cdot}$/$C_3H_3^{\cdot}$ reactive system.[44] While a detailed analysis of the relative yields of different $C_{10}H_8$ isomers is beyond the scope of the present work, Figure 7 shows that two-ring PAHs (plotted as $C_{10}H_8$ 2-ring and mostly consisting of naphthalene, fulvalene, 2-methylene-2*H*-indene, and 5-methylene-5*H*-indene) are not formed by well-skipping reactions in the first part of the reactor but rather from isomerization reactions of five-membered ring species, grouped

https://doi.org/10.1021/acs.jpca.4c02386
J. Phys. Chem. A 2024, 128, 5707−5720

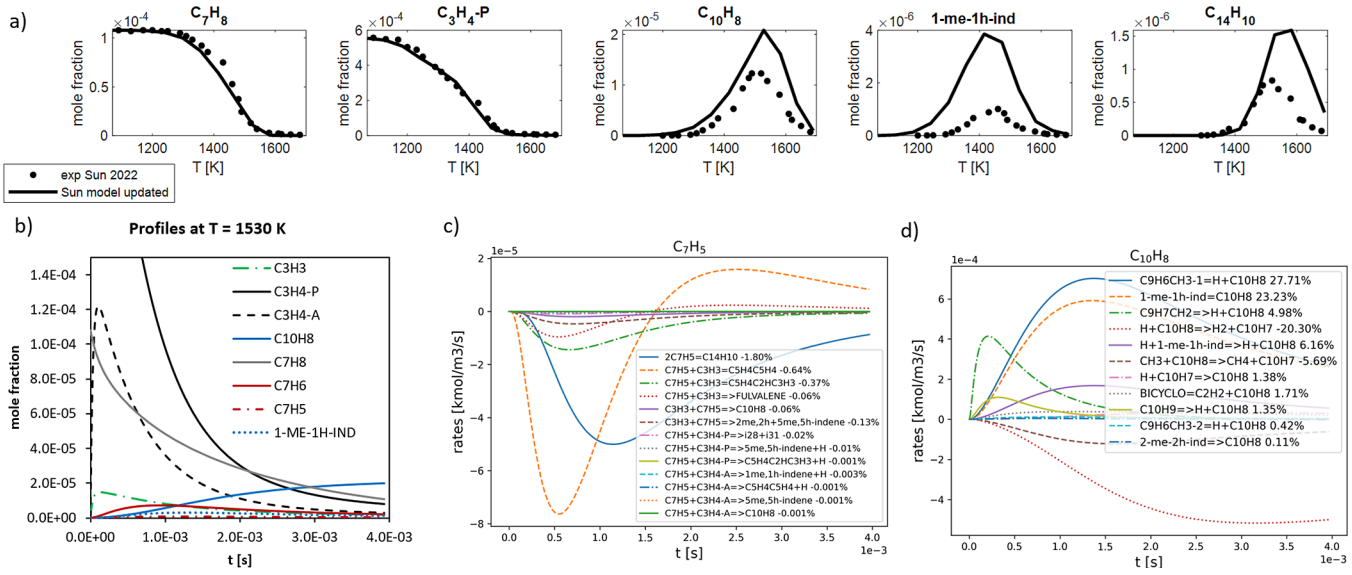

Figure 9. (a) Simulated profiles of the reactants and some relevant PAHs in the shock tube experiments of Sun et al.[50] (b) Profiles of relevant PAHs and species participating in their formation along the ST reactor at 1530 K and reaction rates relevant to the formation and consumption of $C_7H_5^{\cdot}$ and $C_{10}H_8$ (c,d). In (c), the main formation and decomposition pathways are omitted to highlight PAH formation pathways. The % indicates the relative contribution of each reaction to the production/consumption of each species integrated over the residence time in the reactor.

together as $C_5H_4C_2HC_3H_3$ and $C_5H_4C_5H_4$ (see Supporting Information for details). This is highlighted by the reaction rates in Figure 8a, where it is shown that at $t < 1.0 \times 10^{-4}$ s $C_7H_5^{\cdot} + C_3H_3^{\cdot}$ is consumed to $C_5H_4C_2HC_3H_3$ and $C_5H_4C_5H_4$, which are favored at the lower temperatures of this portion of the reactor; then, at longer residence times ($t > 1.0 \times 10^{-3}$ s, Figure 8b,c), $C_5H_4C_2HC_3H_3$ isomers produce some $C_7H_5^{\cdot}$+ $C_3H_3^{\cdot}$ through back-dissociation and are also the main source of naphthalene together with 2-methylene-2*H*-indene. A more accurate evaluation of relative product yields for the $C_7H_5^{\cdot}$ + $C_3H_3^{\cdot}$ reaction will require a careful analysis of branching of its barrierless entrance channels using, for instance, variable reaction coordinate transition state theory (VRC-TST), which was not conducted by Li et al.[44] and will therefore be addressed in a future work. Finally, it might be speculated that the product distribution of the microtubular reactor can also be strongly affected by the secondary chemistry in the presence of abundant Cl atoms, which likely includes Cl-assisted isomerization of $C_{10}H_8$ following a chlorine atom addition and the $C_{10}H_8 + Cl^{\cdot} \rightarrow C_{10}H_7^{\cdot} + HCl$ direct H-abstraction followed by secondary uni- and bimolecular reactions of $C_{10}H_7^{\cdot}$ radicals. When included in the kinetic modeling through rough estimates, the latter pathways also increase the sensitivity of the product distribution to the operating conditions of the reactor. Whereas the kinetics of the $C_7H_5^{\cdot}$ + $C_3H_3^{\cdot}/C_3H_4$ systems is relevant to naphthalene formation in combustion, the secondary Cl-initiated chemistry is not, hence we believe that accurate calculations and kinetic modeling of Cl-assisted isomerization pathways are not of particular interest to the combustion community but rather highlight the shortcomings in the use of chlorinated aromatic precursors in microkinetic experiments.

Figure 9a compares the experimental and simulated profiles of species of interest to this work in the high-pressure shock tube experiments of the copyrolysis of toluene and methylacetylene of Sun et al.[50] Among the detected species, naphthalene and 1-methylene-1*H*-indene, which is supposed to be the main $C_{10}H_8$ product, can be formed from the reaction pathways of $C_7H_5^{\cdot}$ + $C_3H_3^{\cdot}/C_3H_4$ PESs. To assess the relevance of these pathways, species profiles along the reactor at 1530 K (i.e., corresponding to the peaks of two-ring PAHs) are reported in Figure 9b, together with the main reaction rates for the growth of $C_7H_5^{\cdot}$ and naphthalene (Figure 9c,d, respectively). Along the reactor, the concentrations of allene and methylacetylene are substantially larger than those of propargyl radical, thus potentially enhancing the relevance of the molecular pathway. Fulvenallenyl is mainly formed from C_7H_6 dissociation and largely decomposes to small species, such that growth pathways account for only few % of its total reactivity (Figure 9c). At 1530 K, $C_7H_5^{\cdot}$ self-recombination accounts for about 1.8% of its growth, followed by recombination with propargyl (1.4%), addition with methylacetylene (0.03%), and addition with allene (< 0.01%). Also, in this case, the radical pathway largely prevails over the molecular pathway. The relevance of the growth through fulvenallenyl decreases compared to the predictions of the original model, where $C_7H_5^{\cdot} + C_3H_3^{\cdot} \rightarrow C_{10}H_8$/1-methylene-1*H*-indene was highlighted among the main pathways responsible for naphthalene formation.[50] Instead, Figure 9d shows that in the updated model, naphthalene is mostly produced from $C_9H_6CH_3$-1, $C_9H_7CH_2$ (**i18**), and 1-methylene-1*H*-indene isomers, which largely derive from methyl recombination with indenyl. Finally, it is noted that reactions on the $C_7H_5^{\cdot}$ + C_3H_4 PES other than the growth pathways emerge as important in naphthalene production, namely the H-assisted isomerization from 1-methylene-1*H*-indene and the dissociation of the $C_9H_7CH_2$ (**i18**) and $C_9H_6CH_3$-2 (**i33**) isomers. It is noted that the dissociation of $C_9H_6CH_3$-1, which is the main production pathway of naphthalene, is not part of the PES studied in this work. Additionally, while the $C_9H_6CH_3$-2 concentration remains small, this species was newly introduced in the model during this work and its production from other growth channels (e.g., indenyl + methyl) is neglected in the current model and might need to be added. The clarification and the correct description of the reactivity of these $C_{10}H_9$ isomers might have a large impact in

https://doi.org/10.1021/acs.jpca.4c02386
J. Phys. Chem. A 2024, 128, 5707−5720

model predictions. For instance, the present updates produced about a factor of 2 increase in 1-methylene-1*H*-indene compared to the starting model of Sun et al.[50] Hence, the reactivity of $C_{10}H_9$ isomers in combustion kinetic models may need revision.

7. DISCUSSION AND CONCLUSIONS

The reactivity of resonantly stabilized radicals significantly influences the kinetic evolution of many systems, playing, for example, a key role in the formation and growth PAH. It is therefore interesting to determine whether their main reaction pathways involve as coreactant a second radical or a closed-shell species. To answer this question in this work, the reaction of the fulvenallenyl radical with allene and propene was first theoretically and experimentally investigated and then compared with that of propargyl. Electronic structure calculations on the $C_{10}H_9$ PES accessed by the reactions of the fulvenallenyl $C_7H_5^{\cdot}$ radical with C_3H_4 isomers allene and methylacetylene combined with RRKM-ME calculations of $k_{T,p}$ rate constants using the automated EStokTP software suite clearly demonstrate that these reactions are slow. At lower temperatures, the $C_7H_5^{\cdot}$ + allene reaction mostly produces collisionally stabilized $C_{10}H_9$ intermediates, including complexes formed by allene additions to the tail and *ortho* positions in the fulvenallenyl radicals **i1** and **i2** and the subsequent isomer **i4**. The bimolecular $C_{10}H_8$ + H products are formed at higher temperatures, where 1-methylene-1*H*-indene **p8** and naphthalene **p1** are the favored products around 1500 K and 1 atm with relative yields of ∼2.2/1, whereas the direct tail-addition-H-elimination product **p6** takes over at higher temperatures. The collisional stabilization of the $C_{10}H_9$ complexes is even more favored in the $C_7H_5^{\cdot}$ + methylacetylene reaction, where the tail adduct **i24** has the highest branching ratio almost at all considered temperatures. Most favorable $C_{10}H_8$ isomers with significant yields at high temperatures include 5-methylene-5*H*- and 4-methylene-4*H*-indenes **p4** and **p9**, whereas azulene and naphthalene can be produced only in trace amounts, with rate constants on the order of 10^{-19} cm^3 mol^{-1} s^{-1} at 1000 K.

Kinetic modeling of the microtubular reactor allowed us to conclude that the studied molecular growth pathway is noncompetitive with the radical pathway under the present experimental conditions. In fact, propargyl is produced by direct H-abstraction by Cl atoms from allene or methylacetylene. In turn, atomic Cl stems from the pyrolysis of the trichloromethylbenzene precursor. As a result, the concentration of allene and methylacetylene drops in the first instants of the reactor, such that the recombination of fulvenallenyl with propargyl radical prevails due to (1) faster reactivity and (2) extremely low concentrations of C_3H_4 species. Hence, it is noted that in order to probe the reactivity of the $C_7H_5^{\cdot}$ radical experimentally without the interference from secondary Cl-related reactions, a "cleaner" precursor (bonded to atoms less reactive than Cl) needs to be sought. In addition, the competitiveness between the radical and molecular pathways in fulvenallenyl growth was tested under the conditions of the copyrolysis experiments of toluene and methylacetylene of Sun et al.,[50] where the concentration of propargyl radical is at least 1 order of magnitude lower than that of its molecular counterparts. However, also in this case, the contribution of $C_7H_5^{\cdot}$ + propargyl radical to the growth of fulvenallenyl is about 2 orders of magnitude larger than that of $C_7H_5^{\cdot}$ + allene/methylacetylene, thus confirming the small importance of the latter. Nevertheless, the newly computed reaction pathways emerge as relevant, i.e., H-assisted isomerizations between $C_{10}H_8$ isomers and decomposition reactions of various $C_{10}H_9$ isomers. Due to the impact of these updates, a revision of the treatment of $C_{10}H_9$ isomers and their reactivity in combustion kinetic models is recommended.

Overall, our results demonstrate that the fulvenallenyl radical is barely reactive toward allene and methylacetylene, which exemplify unsaturated hydrocarbons−alkenes (more precisely, cumulenes here) and alkynes. The reasons for the slow reactivity include the weakness of the newly formed C−C bond in the addition complexes and the significant entrance barriers, which are typically higher than those for regular localized σ-radicals like phenyl. Saturated hydrocarbons are less reactive than unsaturated ones with respect to radical addition. Moreover, a C−H bond in saturated hydrocarbons, typically, 410−430 kJ mol^{-1}, is much stronger than that in fulvalene, 338 kcal mol^{-1}. This makes the direct H-abstraction channels by fulvenallenyl from saturated hydrocarbons also highly unfavorable thermodynamically. Therefore, the fulvenallenyl radical, once formed, can be consumed only slowly by reactions with closed-shell hydrocarbon molecules. The only possible exception could be the reaction with highly abundant acetylene, which has been recently predicted to produce indenyl radical with a rate constant of few 10^{-15} cm^3 mol^{-1} s^{-1} at prevailing combustion conditions.[78] This leaves unimolecular decomposition as well as oxidation reactions and recombination reactions with other radicals, e.g., $C_3H_3^{\cdot}$, and itself as preferential avenues for the removal of $C_7H_5^{\cdot}$. Hence, as suggested by previous experimental and theoretical investigations, fulvenallenyl reacts slowly, accumulates at high temperatures, and can contribute to the formation of PAHs. Concerning the reaction of fulvenallenyl with propargyl, accurate predictions of its product distribution are still missing in the literature, calling for more detailed theoretical calculations for its PES and, in particular, the branching of the reaction flux among the numerous barrierless entrance channels.

■ ASSOCIATED CONTENT

Supporting Information

The Supporting Information is available free of charge at https://pubs.acs.org/doi/10.1021/acs.jpca.4c02386.

Additional PIE curves; potential energy diagrams illustrating less favorable channels of the $C_7H_5^{\cdot}$ + C_3H_4 reactions; and additional kinetic simulations (DOCX)

Input file for RRKM-ME calculations for the $C_7H_5^{\cdot}$/C_3H_4 system using MESS package (TXT)

Arrhenius fits for the set of lumped rate constants of $C_7H_5^{\cdot}$ + C_3H_4 PES (TXT)

Archived folder containing the temperature- and pressure-dependent composition of the pseudospecies (ZIP)

■ AUTHOR INFORMATION

Corresponding Authors

Alexander M. Mebel − *Department of Chemistry and Biochemistry, Florida International University, Miami, Florida 33199, United States;* orcid.org/0000-0002-7233-3133; Email: mebela@fiu.edu

https://doi.org/10.1021/acs.jpca.4c02386
J. Phys. Chem. A 2024, 128, 5707−5720

Luna Pratali Maffei − *Department of Chemistry, Materials and Chemical Engineering "G. Natta", Politecnico di Milano, 20133 Milano, Italy*; Email: luna.pratali@polimi.it
Long Zhao − *School of Nuclear Science and Technology, University of Science and Technology of China, Hefei, Anhui 230027, China; Deep Space Exploration Laboratory, University of Science and Technology of China, Hefei, Anhui 230026, China*; Email: zhaolong@ustc.edu.cn
Ralf I. Kaiser − *Department of Chemistry, University of Hawaii at Manoa, Honolulu, Hawaii 96888, United States*; orcid.org/0000-0002-7233-7206; Email: ralfk@hawaii.edu

Authors

Wang Li − *National Synchrotron Radiation Laboratory, University of Science and Technology of China, Hefei, Anhui 230029, China*
Carlo Cavallotti − *Department of Chemistry, Materials and Chemical Engineering "G. Natta", Politecnico di Milano, 20133 Milano, Italy*; orcid.org/0000-0002-9229-1401
Alexander N. Morozov − *Department of Chemistry and Biochemistry, Florida International University, Miami, Florida 33199, United States*
Chang-Yang Wang − *National Synchrotron Radiation Laboratory, University of Science and Technology of China, Hefei, Anhui 230029, China*
Jiu-Zhong Yang − *National Synchrotron Radiation Laboratory, University of Science and Technology of China, Hefei, Anhui 230029, China*; orcid.org/0000-0002-7076-3412

Complete contact information is available at: https://pubs.acs.org/10.1021/acs.jpca.4c02386

Author Contributions

[▽]A.M.M. and W.L. contributed equally to this work.

Notes

The authors declare no competing financial interest.

■ ACKNOWLEDGMENTS

The work at Florida International University was supported in part by the US Department of Energy, Basic Energy Sciences DE-FG02-04ER15570. The experimental efforts performed at NSRL were supported by the National Natural Science Foundation of China (22173091). AMM is thankful to Politecnico di Milano for the support of his sabbatical leave stay in Milan and to the members of Cavallotti's and Faravelli's groups for their hospitality. CC acknowledges the support of Italian MUR (PRIN 2020—Grant 202082CE3T) and the CINECA award HP10BCGTXF, under the ISCRA initiative, for the availability of high-performance computing resources. The work at Polimi has been partially supported by ICSC—Centro Nazionale di Ricerca in High Performance Computing, Big Data, and Quantum Computing funded by European Union—NextGenerationEU. L.P.M. work was carried out within the NEST - Network 4 Energy Sustainable Transition (D.D. 1561 11/10/2022, PE00000021) and received funding under the National Recovery and Resilience Plan (NRRP), Mission 4 Component 2 Investment 1.3, funded from the European Union - NextGenerationEU. This manuscript reflects only the authors' views and opinions, neither the European Union nor the European Commission can be considered responsible for them.

■ REFERENCES

(1) Shao, C.; Kukkadapu, G.; Wagnon, S. W.; Pitz, W. J.; Sarathy, S. M. PAH formation from jet stirred reactor pyrolysis of gasoline surrogates. *Combust. Flame* **2020**, *219*, 312−326.
(2) Kukkadapu, G.; Wagnon, S.; Pitz, W.; Hansen, N. Identification of the molecular weight growth reaction network in counterflow flames of the C_3H_4 isomers allene and propyne. *Proc. Combust. Inst.* **2021**, *38*, 1477−1485.
(3) Hansen, N.; Yang, B.; Braun-Unkhoff, M.; Ramirez, A.; Kukkadapu, G. Molecular-growth pathways in premixed flames of benzene and toluene doped with propyne. *Combust. Flame* **2022**, *243*, No. 112075.
(4) Langer, R.; Mao, Q.; Pitsch, H. A detailed kinetic model for aromatics formation from small hydrocarbon and gasoline surrogate fuel combustion. *Combust. Flame* **2022**, *245*, No. 112574.
(5) Silva, G. d.; Bozzelli, J. W. The C_7H_5 fulvenallenyl radical as a combustion intermediate: Potential new pathways to two- and three-ring PAHs. *J. Phys. Chem. A* **2009**, *113*, 12045−12048.
(6) Haynes, B. S.; Wagner, H. G. Soot formation. *Prog. Energy Combust. Sci.* **1981**, *7*, 229−273.
(7) Wagner, H. G. Soot formation in combustion. *Proc. Combust. Inst.* **1979**, *17*, 3−19.
(8) Frenklach, M. Reaction mechanism of soot formation in flames. *Phys. Chem. Chem. Phys.* **2002**, *4*, 2028−2037.
(9) Frenklach, M.; Mebel, A. M. On the mechanism of soot nucleation. *Phys. Chem. Chem. Phys.* **2020**, *22*, 5314−5331.
(10) Cataldo, F.; García-Hernández, D. A.; Manchado, A. Coal and other organics in space. *Astrophys. Space Sci.* **2020**, *365*, 5−18.
(11) Cherchneff, I. The formation of polycyclic aromatic hydrocarbons in evolved circumstellar environments. *EAS Publications Series* **2011**, *46*, 177−189.
(12) Ruth, A. A.; Kim, E. K.; Hese, A. The S_0-S_1 cavity ring-down absorption spectrum of jet-cooled azulene: Dependence of internal conversion on the excess energy. *Phys. Chem. Chem. Phys.* **1999**, *1*, 5121−5128.
(13) van der Zwet, G. P.; Allamandola, L. J. Polycyclic aromatic hydrocarbons and the diffuse interstellar bands. *Astron. Astrophys.* **1985**, *146*, 76−80.
(14) Mebel, A. M.; Landera, A.; Kaiser, R. I. Formation mechanisms of naphthalene and indene: From the interstellar medium to combustion flames. *J. Phys. Chem. A* **2017**, *121*, 901−926.
(15) Kaiser, R. I.; Hansen, N. An aromatic universe-A physical chemistry perspective. *J. Phys. Chem. A* **2021**, *125*, 3826−3840.
(16) Frenklach, M.; Clary, D. W.; Gardiner, W. C.; Stein, S. E. Detailed kinetic modeling of soot formation in shock-tube pyrolysis of acetylene. *Proc. Combust. Inst.* **1985**, *20*, 887−901.
(17) Frenklach, M. On the driving force of PAH production. *Proc. Combust. Inst.* **1989**, *22*, 1075−1082.
(18) Parker, D. S.; Kaiser, R. I.; Troy, T. P.; Ahmed, M. Hydrogen Abstraction/Acetylene Addition Revealed. *Angew. Chem., Int. Ed. Engl.* **2014**, *53*, 7740−7744.
(19) Yang, T.; Troy, T. P.; Xu, B.; Kostko, O.; Ahmed, M.; Mebel, A. M.; Kaiser, R. I. Hydrogen-abstraction/acetylene-addition exposed. *Angew. Chem., Int. Ed.* **2016**, *55*, 14983−14987.
(20) Mebel, A. M.; Georgievskii, Y.; Jasper, A. W.; Klippenstein, S. J. Temperature- and pressure-dependent rate coefficients for the HACA pathways from benzene to naphthalene. *Proc. Combust. Inst.* **2017**, *36*, 919−926.
(21) Parker, D. S.; Zhang, F.; Kim, Y. S.; Kaiser, R. I.; Landera, A.; Kislov, V. V.; Mebel, A. M.; Tielens, A. G. Low temperature formation of naphthalene and its role in the synthesis of PAHs (polycyclic aromatic hydrocarbons) in the interstellar medium. *Proc. Natl. Acad. Sci. U.S.A.* **2012**, *109*, 53−58.
(22) Zhao, L.; Kaiser, R. I.; Xu, B.; Ablikim, U.; Ahmed, M.; Zagidullin, M. V.; Azyazov, V. N.; Howlader, A. H.; Wnuk, S. F.; Mebel, A. M. VUV photoionization study of the formation of the simplest polycyclic aromatic hydrocarbon: Naphthalene ($C_{10}H_8$). *J. Phys. Chem. Lett.* **2018**, *9*, 2620−2626.

(23) Melius, C. F.; Colvin, M. E.; Marinov, N. M.; Pitz, W. J.; Senkan, S. M. Reaction mechanisms in aromatic hydrocarbon formation involving the C_5H_5 cyclopentadienyl moiety. *Proc. Combust. Inst.* **1996**, *26*, 685−692.
(24) Kislov, V. V.; Mebel, A. M. The formation of naphthalene, azulene, and fulvalene from cyclic C_5 species in combustion: An ab initio/RRKM study of 9-H-fulvalenyl (C_5H_5-C_5H_4) radical rearrangements. *J. Phys. Chem. A* **2007**, *111*, 9532−9543.
(25) Cavallotti, C.; Polino, D. On the kinetics of the C_5H_5+C_5H_5 reaction. *Proc. Combust. Inst.* **2013**, *34*, 557−564.
(26) Long, A. E.; Merchant, S. S.; Vandeputte, A. G.; Carstensen, H. H.; Vervust, A. J.; Marin, G. B.; Geem, K. M. V.; Green, W. H. Pressure dependent kinetic analysis of pathways to naphthalene from cyclopentadienyl recombination. *Combust. Flame* **2018**, *187*, 247−256.
(27) Kaiser, R. I.; Zhao, L.; Lu, W.; Ahmed, M.; Zagidullin, M. V.; Azyazov, V. N.; Mebel, A. M. Gas-phase formation of benzene (C_6H_6) and naphthalene ($C_{10}H_8$) through resonantly stabilized cyclopentadienyl-mediated radical-radical reactions. *J. Phys. Chem. Lett.* **2022**, *13*, 208−213.
(28) Matsugi, A.; Miyoshi, A. Computational study on the recombination reaction between benzyl and propargyl radicals. *Int. J. Chem. Kinet.* **2012**, *44*, 206−218.
(29) He, C.; Kaiser, R. I.; Lu, W.; Ahmed, M.; Krasnoukhov, V. S.; Pivovarov, P. S.; Zagidullin, M. V.; Azyazov, V. N.; Morozov, A. N.; Mebel, A. M. Unconventional gas-phase preparation of the prototype polycyclic aromatic hydrocarbon naphthalene ($C_{10}H_8$) via the reaction of benzyl (C_7H_7) and propargyl (C_3H_3) radicals coupled with hydrogen-atom assisted isomerization. *Chem. Sci.* **2023**, *14*, 5369−5378.
(30) Mebel, A. M.; Georgievskii, Y.; Jasper, A. W.; Klippenstein, S. J. Pressure-dependent rate constants for PAH growth: Formation of indene and its conversion to naphthalene. *Faraday Discuss.* **2016**, *195*, 637−670.
(31) Zhao, L.; Kaiser, R. I.; Lu, W.; Xu, B.; Ahmed, M.; Morozov, A. N.; Mebel, A. M.; Howlader, A. H.; Wnuk, S. F. Molecular mass growth through ring expansion in polycyclic aromatic hydrocarbons via radical-radical reactions. *Nat. Commun.* **2019**, *10*, 3689.
(32) Dong, S.; Wagnon, S. W.; Pratali Maffei, L.; Kukkadapu, G.; Nobili, A.; Mao, Q.; Pelucchi, M.; Cai, L.; Zhang, K.; Raju, M.; Chatterjee, T.; Pitz, W. J.; Faravelli, T.; Pitsch, H.; Senecal, P. K.; Curran, H. J. A new detailed kinetic model for surrogate fuels: C3MechV3.3. *Appl. Energy Combust. Sci.* **2022**, *9*, No. 100043.
(33) Alarcon, J. F.; Morozov, A. N.; Mebel, A. M.; Della Libera, A.; Pratali Maffei, L.; Cavallotti, C. Mechanism and kinetics of the oxidation of propargyl radical by atomic oxygen. *Proc. Combust. Inst.* **2024**, *40*, 105372
(34) Langer, R.; Mao, Q.; Pitsch, H. A detailed kinetic model for aromatics formation from small hydrocarbon and gasoline surrogate fuel combustion. *Combust. Flame* **2023**, *258*, No. 112574.
(35) Jin, H.; Farooq, A. C_7 reaction mechanism and its self-imitation in the kinetic modeling of PAH formation. *Combust. Flame* **2023**, *253*, No. 112816.
(36) Polino, D.; Cavallotti, C. Fulvenallene decomposition kinetics. *J. Phys. Chem. A* **2011**, *115*, 10281−10289.
(37) da Silva, G. Reaction of benzene with atomic carbon: Pathways to fulvenallene and the fulvenallenyl radical in extraterrestrial atmospheres and the interstellar medium. *J. Phys. Chem. A* **2014**, *118*, 3967−3972.
(38) He, C.; Thomas, A. M.; Galimova, G. R.; Morozov, A. N.; Mebel, A. M.; Kaiser, R. I. Gas-phase formation of fulvenallene (C_7H_6) via the Jahn-Teller distorted tropyl (C_7H_7) radical intermediate under single-collision conditions. *J. Am. Chem. Soc.* **2020**, *142*, 3205−3213.
(39) Cavallotti, C.; Derudi, M.; Rota, R. On the mechanism of decomposition of the benzyl radical. *Proc. Combust. Inst.* **2009**, *32*, 115−121.
(40) Derudi, M.; Polino, D.; Cavallotti, C. Toluene and benzyl decomposition mechanisms: Elementary reactions and kinetic simulations. *Phys. Chem. Chem. Phys.* **2011**, *13*, 21308−21318.
(41) Cernicharo, J.; Fuentetaja, R.; Agúndez, M.; Kaiser, R. I.; Cabezas, C.; Marcelino, N.; Tercero, B.; Pardo, J. R.; de Vicente, P. Discovery of fulvenallene in TMC-1 with the QUIJOTE line survey. *Astron. Astrophys.* **2022**, *663*, L9.
(42) Jin, H.; Xing, L.; Yang, J.; Zhou, Z.; Qi, F.; Farooq, A. Continuous butadiyne addition to propargyl: A radical-efficient pathway for polycyclic aromatic hydrocarbons. *J. Phys. Chem. Lett.* **2021**, *12*, 8109−8114.
(43) He, Y.; Chen, J.; Zheng, X.; Xu, X.; Li, W.; Yang, L.; Tian, W. Spiral graphene nanoribbons with azulene defects as potential nonlinear optical materials. *ACS Appl. Nano. Mater.* **2019**, *2*, 1648−1654.
(44) Li, W.; Yang, J.; Zhao, L.; Couch, D.; Marchi, M. S.; Hansen, N.; Morozov, A. N.; Mebel, A. M.; Kaiser, R. I. Gas-phase preparation of azulene ($C_{10}H_8$) and naphthalene ($C_{10}H_8$) via the reaction of the resonantly stabilized fulvenallenyl and propargyl radicals. *Chem. Sci.* **2023**, *14*, 9795−9805.
(45) Costa, A.; López-Castillo, A. Prediction of azulene-based nanographene-like materials. *Diam. Relat. Mater.* **2021**, *112*, No. 108235.
(46) Ogawa, N.; Yamaoka, Y.; Takikawa, H.; Yamada, K. I.; Takasu, K. Helical nanographenes embedded with contiguous azulene units. *J. Am. Chem. Soc.* **2020**, *142*, 13322−13327.
(47) Zheng, X.; Liu, L.; Yang, C.; He, Y.; Chen, J.; Tian, W. Modulation of the second order nonlinear optical properties of helical graphene nanoribbons through introducing azulene defects or/and BN units. *Chem. Res. Chin. Univ.* **2022**, *38*, 974−984.
(48) Li, W.; Zhao, L.; Kaiser, R. I. A unified reaction network on the formation of five-membered ringed polycyclic aromatic hydrocarbons (PAHs) and their role in ring expansion processes through radical-radical reactions. *Phys. Chem. Chem. Phys.* **2023**, *25*, 4141−4150.
(49) Zhou, Z.; Du, X.; Yang, J.; Wang, Y.; Li, C.; Wei, S.; Du, L.; Li, Y.; Qi, F.; Wang, Q. The vacuum ultraviolet beamline/endstations at NSRL dedicated to combustion research. *J. Synchrotron Radiat.* **2016**, *23*, 1035−45.
(50) Sun, W.; Hamadi, A.; Abid, S.; Chaumeix, N.; Comandini, A. Influences of propylene/propyne addition on toluene pyrolysis in a single-pulse shock tube. *Combust. Flame* **2022**, *236*, No. 111799.
(51) Hansen, N.; Skeen, S. A.; Michelsen, H. A.; Wilson, K. R.; Kohse-Hoinghaus, K. Flame experiments at the advanced light source: New insights into soot formation processes. *J. Vis. Exp.* **2014**, *87*, No. e51369.
(52) Johnson, M.; Bodi, A.; Schulz, L.; Gerber, T. Vacuum ultraviolet beamline at the Swiss Light Source for chemical dynamics studies. *Nuclear Instruments and Methods in Physics Research Section A: Accelerators, Spectrometers, Detectors and Associated Equipment* **2009**, *610*, 597−603.
(53) Golan, A.; Ahmed, M. Molecular beam mass spectrometry with tunable vacuum ultraviolet (VUV) synchrotron radiation. *J. Vis. Exp.* **2012**, *68*, No. e50164.
(54) Cavallotti, C.; Pelucchi, M.; Georgievskii, Y.; Klippenstein, S. J. EStokTP: Electronic structure to temperature- and pressure-dependent rate constants—A code for automatically predicting the thermal kinetics of reactions. *J. Chem. Theory Comput.* **2019**, *15*, 1122−1145.
(55) Frisch, M. J.; Trucks, G. W.; Schlegel, H. B.; Scuseria, G. E.; Robb, M. A.; Cheeseman, J. R.; Scalmani, G.; Barone, V.; Mennucci, B.; Petersson, G. A.; et al.*Gaussian 09, revision B.01*; Gaussian, Inc.: Wallingford CT, 2010.
(56) Kállay, M.; Nagy, P. R.; Mester, D.; Rolik, Z.; Samu, G.; Csontos, J.; Csóka, J.; Szabó, P. B.; Gyevi-Nagy, L.; Hégely, B. The MRCC program system: Accurate quantum chemistry from water to proteins. *J. Chem. Phys.* **2020**, *152*, No. 074107.
(57) *Mrcc, A Quantum Chemical Program Suite* written by Kállay, M.; Nagy, P. R.; Mester, D.; Gyevi-Nagy, L.; Csóka, J.; Szabó, P. B.; Rolik, Z.; Samu, G.; Csontos, J.; Hégely, B., et al.See www.mrcc.hu.

https://doi.org/10.1021/acs.jpca.4c02386
J. Phys. Chem. A 2024, 128, 5707−5720

(58) Chai, J. D.; Head-Gordon, M. Long-range corrected hybrid density functionals with damped atom-atom dispersion corrections. *Phys. Chem. Chem. Phys.* **2008**, *10*, 6615−6620.
(59) Kállay, M.; Horváth, R. A.; Gyevi-Nagy, L.; Nagy, P. R. Basis set limit CCSD(T) energies for extended molecules via a reduced-cost explicitly correlated approach. *J. Chem. Theory Comput.* **2023**, *19*, 174−189.
(60) Dunning, T. H. J. Gaussian basis sets for use in correlated molecular calculations. I. The atoms boron through neon and hydrogen. *J. Chem. Phys.* **1989**, *90*, 1007−1023.
(61) Martin, J. M. L.; Uzan, O. Basis set convergence in second-row compounds. The importance of core polarization functions. *Chem. Phys. Lett.* **1998**, *282*, 16−24.
(62) Georgievskii, Y.; Miller, J. A.; Burke, M. P.; Klippenstein, S. J. Reformulation and solution of the master equation for multiple-well chemical reactions. *J. Phys. Chem. A* **2013**, *117*, 12146−1215.
(63) Georgievskii, Y.; Klippenstein, S. J. *MESS Program Package*, https://tcg.cse.anl.gov/papr: 2020. Accessed on Jun. 8, 2024.
(64) Troe, J. Theory of thermal unimolecular reactions at low pressures. I. Solutions of the master equation. *J. Chem. Phys.* **1977**, *66*, 4745−4757.
(65) Jasper, A. W.; Oana, C. M.; Miller, J. A. Third-body collision efficiencies from combustion modeling: Hydrocarbons in atomic and diatomic baths. *Proc. Combust. Inst.* **2015**, *35*, 197−204.
(66) Frenklach, M.; Singh, R. I.; Mebel, A. M. On the low-temperature limit of HACA. *Proc. Combust. Inst.* **2019**, *37*, 969−976.
(67) Farrell, J. T.; Taatjes, C. A. Infrared frequency-modulation probing of Cl+C_3H_4 (allene, propyne) reactions: Kinetics of HCl production from 292 to 850 K. *J. Phys. Chem. A* **1998**, *102*, 4846−4856.
(68) Pelucchi, M.; Frassoldati, A.; Faravelli, T.; Ruscic, B.; Glarborg, P. High-temperature chemistry of HCl and Cl_2. *Combust. Flame* **2015**, *162*, 2693−2704.
(69) Miller, J. A.; Klippenstein, S. J. The recombination of propargyl radicals and other reactions on a C_6H_6 potential. *J. Phys. Chem. A* **2003**, *107*, 7783−7799.
(70) Pratali Maffei, L.; Pelucchi, M.; Cavallotti, C.; Bertolino, A.; Faravelli, T. Master equation lumping for multi-well potential energy surfaces: A bridge between ab initio based rate constant calculations and large kinetic mechanisms. *Chem. Eng. J.* **2021**, *422*, No. 129954.
(71) Zagidullin, M. V.; Kaiser, R. I.; Porfiriev, D. P.; Zavershinskiy, I. P.; Ahmed, M.; Azyazov, V. N.; Mebel, A. M. Functional relationships between kinetic, flow, and geometrical parameters in a high-temperature chemical microreactor. *J. Phys. Chem. A* **2018**, *122*, 8819−8827.
(72) Cuoci, A.; Frassoldati, A.; Faravelli, T.; Ranzi, E. OpenSMOKE ++: An object-oriented framework for the numerical modeling of reactive systems with detailed kinetic mechanisms. *Comput. Phys. Commun.* **2015**, *192*, 237−264.
(73) Jin, H.; Yang, J.; Farooq, A. Determination of absolute photoionization cross-sections of some aromatic hydrocarbons. *Rapid Commun. Mass Spectrom.* **2020**, *34*, No. e8899.
(74) Palmer, M. H.; Coreno, M.; Simone, M. d.; Grazioli, C.; Jones, N. C.; Hoffmann, S. V.; Aitken, R. A. The ground and ionized states of azulene: A combined study of the vibrational energy levels by photoionization, configuration interaction, and density functional calculations. *J. Chem. Phys.* **2022**, *156*, No. 064305.
(75) Jochims, H. W.; Rasekh, H.; Ruhl, E.; Baumgartel, H.; Leach, S. The photofragmentation of naphthalene and azulene monocations in the energy range 7−22 eV. *Chem. Phys.* **1992**, *168*, 159−184.
(76) Steinbauer, M.; Hemberger, P.; Fischer, I.; Bodi, A. Photoionization of C_7H_6 and C_7H_5: Observation of the fulvenallenyl radical. *ChemPhysChem* **2011**, *12*, 1795−7.
(77) Ruscic, B.; Bross, D. H. Active Thermochemical Tables (ATcT) values based on ver. 1.130 of the Thermochemical Network, 2022; available at ATcT.anl.gov.
(78) Jin, H.; Mebel, A. M.; Farooq, A. Acetylene addition to the fulvenallenyl moiety in aromatic hydrocarbons. *Proc. Combust. Inst.* **2024**, *40*, submitted.

https://doi.org/10.1021/acs.jpca.4c02386
J. Phys. Chem. A 2024, 128, 5707−5720